

CG lightning and cloud-top-temperature over the contiguous United States.

G. Molinie

Space and Atmospheric Sciences Group, Los Alamos National Laboratory,
Los Alamos, New Mexico, USA

A. R. JACOBSON

Space and Atmospheric Sciences Group, Los Alamos National Laboratory,
Los Alamos, New Mexico, USA

G. Molinie, Space and Atmospheric Sciences Group, Los Alamos National Laboratory, Los Alamos, New Mexico, USA (gmolinie@lanl.gov)

Abstract. This study analyzes cloud-top-temperature (CTT) and lightning stroke densities (CG densities) over the CONUS from May to October 1999. A large number of co-located stroke densities and CTT are available, providing robust statistics.

This work shows that thunderstorms can be classified into two sets :

1. Those with CTT warmer than -55°C that constitute 80 % of the observed $\pm\text{CGs}$. For these storms, overall CG densities are quasi-constant whatever CTT .
2. Those with CTT colder than -55°C for which the CG densities increase as CTT decreases. This is in good agreement with the current knowledge on links between convective vigors and cloud-electrification levels.

Moreover, a region by region study reveals the latitude dependence of the CG stroke densities. The higher the latitude, the lower are the $\pm\text{CG}$ densities. The latitude dependence of the CG densities is discussed in terms of tropopause height.

1. Introduction

The two main lightning types produced in thunderclouds are intra-cloud (IC) and cloud-to-ground (CG) flashes. IC is usually the prevalent type, although the ratio IC:CG can vary dramatically from one cloud to another. *Chèze and Sauvageot* [1997] show that the ratio IC:CG can range from 0.5 to 70, but only 2 storms out of 60 their had IC:CG ratio lower than 1.

Nevertheless, CG the lightning type that has been most studied during the last 10 or 15 years, at least via field observations. A reason is the installation, in several countries, of networks for automated detection of CG lightning. In USA, for example, a network called NLDN (National Lightning Detection Network) consists of both direction finder (DF) type and LPATS (Lightning Position and Tracking System) based on the Time-Of-Arrival technique (TOA) sensors [*Orville, 1991*], [*Orville, 1994*], [*Orville and Silver, 1997*], and, [*Huffines and Orville, 1999*]. In Canada, such a network is also installed : the CLDN (Canadian Lightning Detection Network) using both a technique called IMPACT/ES (Improved Accuracy from Combined Technology / Enhanced Sensitivity) and LPATS. France is covered with a DF system [*Tourte et al., 1988*], as are Finland, Japan (JLDN), Australasia (TOGA Lightning Location Network). LPATS arrays are installed for example in Germany [*Fister et al.*] and Switzerland [*Rubinstein et al.*].

The cloud-top-temperature (CTT) is also a parameter routinely acquired all around the world by geostationary satellites [*Johnson et al., 1994*]. The United States maintains two satellites covering the Atlantic and the Pacific Ocean, called GOES-EAST and GOES-WEST. They are currently equivalent to GOES-8 and GOES-10, respectively situated at longitude 75°W and 135 °W. The European Space Agency operates METEOSAT satellites

deployed along the Greenwich meridian and over the Atlantic ocean . There is also a Japanese geostationary satellite called GMS, deployed over the Pacific ocean, and an Indian one positioned at 74 °E.

Thundercloud electrification is believed to be due mainly to ice-ice collisions [*Takahashi*, 1978; *Jayaratne et al.*, 1983; *Gardiner et al.*, 1985]. The convective vigor of thunderclouds, is one of the main factors driving the magnitude of their electrification (see *Williams* [2001] for a review of this topic). The more intense the updrafts, the more they carry air above the freezing level, producing both large ice particles and supercooled liquid water, thereby promoting cloud electrification. CGs are divided into two categories : - CGs carrying a negative charge to ground and +CGs carrying a positive charge. - CGs constitute the major part of CGs in most (but not all) storms. Typically, they connect the main negative cloud charge to the ground. They are associated with the descent of precipitating ice particles, and their occurrence is favored by a positive charged region near the cloud base [*Goodman, Buechler, and Wright*, 1988; *Williams, Weber, and Orville*, 1989; *Carey and Rutledge*, 1996]. +CGs have many different origins depending on which kind of storm they occur in. They often propagate from the lower positive charge center in isolated convective storm or in severe hail storms [*MacGorman and Burgess*, 1994; *Carey and Rutledge*, 1998]. They start in a tilted upper positive charge in MCS (Mesoscale Convective System) [*Parker et al.*, 2001], or from positive charge advected over long distance or locally produced in MCS anvils [*Rutledge and MacGorman*, 1988; *Stolzenburg*, 1990; *Zajac and Rutledge*, 2001]. +CGs often are detected during or around the occurrence of severe weather (hail, tornado) and may neutralize the positive charge carried by large hail particles [*Perez et al.*, 1997; *Williams et al.*, 1999; *Kane*, 1991].

Light ice particles are situated at the top of the thundercloud. They are usually produced in the updraft and carried to the cloud top where they remain because they are too light to precipitate. Their altitude and their concentration depend on the convective vigor of the thundercloud. Moreover, the non-precipitating small ice particles can be advected to the top of thundercloud anvil, and then the “memory” of the updraft vigor of the convective cell remains. *Liu and Curry* [1998] showed that the ice water path (the column integrated ice water content, *Sheu et al.* [1997]) and CTT (measured at $12\mu\text{m}$) were correlated in tropical clouds.

Both CTT and CG activity levels depend grossly on the ice phase and convective vigor of the thundercloud. Databases of these two parameters (CTT and CG) are available all around the globe. This article describes their systematic inter-comparison over the CONUS. *Vonnegut* [1963], *Williams* [1985] and *Williams* [2001] reported a scaling relation between the total flash rate and the convective vigor of thunderclouds. *Price and Rind* [1992] used such a relation to elaborate a global lightning parameterization as a function of the cloud-top height. Such scaling relations are important because they allow us to adjust model results and more specifically to deduce lightning flash rate from meteorological parameters like the cloud-top-height in implicitly-resolving cloud models. One application is LNO_x (Lightning produced NO_x) concentration computation from CTT (*Price et al.* [1997],...) for example. The parameterization of *Price and Rind* [1992] has often been used in such work.

Questions remain regarding the range of validity of CTT/CG density scaling laws. Is such a scaling law valid for the particular case of CGs when we ignore ICs? Studies on CGs reported in *MacGorman et al.* [1989] or *Lang and Rutledge* [2002] question whether there

should be a monotonic increase of the CG rate with an increase of the size of thunderclouds. Indeed, the more intense the updrafts, the larger are thunderclouds and thus the larger are the gaps between the main negative charge center and the lower positive charge zone near the cloud base. The competition between the cloud electrification enhancement, and the -CG-triggering probability decrease, leads to a decrease of the -CG rate in the tallest thunderstorms (mechanism called “ charge elevated mechanism”). *Ushio et al.* [2001] addressed this issue via a statistical study comparing cloud-top height and total flash rate, both detected from space. They stated : “the fifth power dependency that is derived from scaling laws is not inconsistent with, but not necessarily required by, the observed data.”

In the following, we compare CG lightning data from NLDN and CTT inferred from GOES-8 data. Both data sets are routinely available. Data from May to October 1999 are involved in this study. In the next section, the two databases, NLDN and GOES-8 are presented, followed by an overall analysis of the stroke densities and associated CTT. Then, stroke density and CTT correspondences are detailed month-by-month and region-by-region. Probability of CG occurrences and overall stroke density are computed as functions of CTT.

2. The Data

2.1. Cloud-Top Temperature

CTT are retrieved from the infrared $10.7 \mu m$ channel of the GOES-8 satellite. Data used cover a period extending from May to October 1999 inclusive. These data are discretized in temperature bins. The CTT ranges from +35 to -80 °C. Electrical charge densities consistent with the lightning stage in clouds are mainly carried by ice particles [*Gardiner*

et al., 1985; *Weinheimer et al.*, 1991]. The regions in thunderclouds where ice particle collisions lead to cloud electrification are situated between -10 and -20 °C [*Dye et al.*, 1986]. As the cloud top will be always at colder temperature than the region of cloud electrification, the lowest bin boundary is chosen at -10 °C to be sure that we include all thundercloud CTT conditions in our study. Few CTT are expected between -10 and -15 °C. Thus the first temperature bin runs from -10 to -20 °C. However, the other CTT bins are 5 °C wide and range over -20 to -80 °C. Hereafter, these CTT bins are called regular CTT bins.

The geographic cells, in which CTT data in this study are discretized, are chosen to coincide with the GOES-8 grid. The size of the mesh grid along meridians and parallels increases with latitude, and somewhat with west longitude over North America. Over CONUS, the mesh size increases from 10 km at the South East to 20 km at the North West. Between latitudes 30 °N and 50 °N, that is, over the major part of the domain studied, the mesh grid is roughly between 11 and 15 km wide in each direction.

2.2. The Stroke Density Data Base

The lightning data used in this study are derived from the NLDN data for May to October 1999 inclusive. The NLDN network consists of more than 100 sensors including both direction finders and TOA sensors. Data obtained from this network are fully described in particular in *Orville [1991]*, *Orville [1994]*, *Cummins et al. [1998]*, *Orville and Silver [1997]*, *Huffines and Orville [1999]*, *Orville et al. [2002]*. NLDN data include the geolocation, date, time, peak current and the classification of strokes as cloud (IC) or ground stroke (CG). The sign of the peak current gives the CG polarity. In the available dataset only the -CG and +CG classification of lightning strokes are guaranteed. Thus,

only these data are used in the current study. *Cummins et al.* [1998] reported that over the contiguous United States of America, the CG detection efficiency is around 80 – 90% since 1994, and *Idone et al.* [1998] estimated the median accuracy of the lightning location at 500 m.

As the amount of data is large, -CG and +CG stroke densities are computed in 15-min epochs and in area elements matching the GOES-8 grid, this means a slightly different grid day-to-day, due to the satellite positioning adjustment. The stroke density data are then binned as described in the following.

2.2.1. Flash or stroke density. Positive CGs are on average less numerous than -CGs by about a factor 10. For the year 1999, *Orville et al.* [2002] found yearly maxima of +CG density of about 0.7 *stroke/km²/h* over the United States and of about 9 *stroke/km²/h* for -CGs. Thus, we can expect to have different orders of magnitude for densities of the two polarities of CGs. Two different discretization ranges are therefore necessary: for -CGs, the discretization bin upper boundaries (Fd1) are given by $Fd1 = 0.1 \times \exp(0.53j)$ where j is the bin index varying from 1 to 11. ; for + CGs, the bin higher boundaries (Fd2) are given by $Fd2 = 0.01 \times \exp(0.53j)$ where j is the bin index varying from 1 to 11. The lowest limit of the two Fd ranges (lower boundary of the first bin) is set to $Fd1(0) = Fd2(0) = 0.001 \text{ stroke}/15mn / km^2$ in order to include the lowest flash or stroke density one can differentiate from zero. The maximum grid size is about 400 *km²*. If, during a 15 minute period, there is one lightning occurring in such a grid, that is a density of 0.0025 *stroke/15mn / km²*. Thus, with the lowest boundary at 0.001 *stroke/15mn / km²*, we are sure to include stroke or flash densities due to only one lightning event per 15 minutes, in a grid of area equal to or lower than 400 *km²*.

2.2.2. Region and time-period divisions. The CG/CTT correspondences are computed in different geographic areas and for different local time periods. Days are divided in 3 local time periods : 8:00 to 14:00 ; 14:00 to 21:00 and 21:00 to 8:00. The domain of computation is limited to the CONUS, where the NLDN detection efficiency is greater than 80% [Cummins et al., 1998] in 1999. In order to study parameters possibly affecting CTT/stroke density correspondences, the study domain is divided into 5 zones, drawn in figure 1. Region 1 corresponds to the highest latitude of the study domain and regions where both +CG and -CG densities are among the lowest in the U.S.A. in 1999 [Orville et al., 2002]. Orville et al. shows also that the Gulf coast and Florida display among the highest +CGs and -CGs densities in 1998 and 1999, these regions are numbered 2 and 5 respectively. Region 3 is a continental region frequently displaying high +CG and -CGs densities. This area includes the Midwest, where mesoscale convective systems (MCS) occur. Finally, Region 4 includes the Rocky Mountain range and adjacent high plains. Orville et al. showed that the area corresponding to region 4 exhibits quasi-uniform +CG and -CGs densities in 1999. Zone 0 is the whole study domain, the total of zones 1 through 4.

2.3. CTT/ Stroke-Density Correspondences

Lightning flashes are the result of electric-field enhancement due to high electric charge densities. High electric charge densities are generated in convective cells of about 10-km horizontal dimension. Lightning occurrence is often reported at several kilometers or tens of kilometers from the convective cell, (see e. g. [MacGorman and Rust, 1998]). Thus, owing to the possible location of convective cells near the edge of a grid mesh or to lightning associated with cloud anvils, lightning may occur at locations where the cloud

is not directly responsible of the electric-charge generation that supplies the lightning. As an attempt to correct this bias, the CTT is taken as the minimum value of the CTT in the 9 GOES-8 pixels surrounding and including the geolocation of strokes.

2.4. Statistical Weight of the Study

The statistical reliability of this study depends on the number of events used. Thus, the number of CTT/stroke density pairs taken into account each month, in each category of lightning, are reported in table 1. +CG are from 0.7 to 3.2 million of events each month and -CG are between 2.6 and 16 million each month. For these data, the month when the events are the most numerous is June, followed by August, May, July , September and October. From September to October the number of events in each category decreases sharply (by a factor 4 or 5). Moreover, we note that the ratio +GC:-CG lies between 0.2 and 0.3.

In figures 2 and 3 are plotted the number of pixels (i.e. GOES-8 grid meshes) where, respectively, the -CG and the +CG stroke densities are positive, for each regular CTT bin. In the part of the study where regions and months are distinguished, data of July and August are combined as their behavior are similar. That combining of two months increases the confidence one can have in the statistics for these months, because of the large number of events that behave similarly. In all regions, except regions 1, and for each month, except October, the number of available pixels displays a sharp decrease for CTT colder than -60°C , for both -CGs and +CGs. This is due to the number of available CTT points colder than -60°C , rather than to an efficiency of very cloud-top thunderclouds in producing lightning. For temperatures warmer than -60°C the number of events in regions 0, 2, 3, 4 and 5 from May to September 1999 is always sufficient (greater than 1000) to

ensure statistical reliability. For CTT colder than $-60\text{ }^{\circ}\text{C}$, the number of events is usually sufficient for reliable statistics. The one statistically marginal month, October, shows particularly few pixels at cold temperatures. The decrease of available pixels containing either $-CG$ or $+CG$ occurs around $-40\text{ }^{\circ}\text{C}$ in October. However, for CTT warmer than $-55\text{ }^{\circ}\text{C}$, the number of pixels is always greater than 100, which is at least adequate for statistical purposes.

3. CTT/Stroke-Density Distribution

In this section, we analyse the distribution of CTT/stroke-density pairs for the overall data set spanning from May to October 1999. CTT is divided into four broad temperature bins covering the range -10 to $-80\text{ }^{\circ}\text{C}$. The first of these bins runs from -10 to $-35\text{ }^{\circ}\text{C}$, the others are $15\text{ }^{\circ}\text{C}$ wide and thus covering the bins -35 to $-50\text{ }^{\circ}\text{C}$, -50 to $-65\text{ }^{\circ}\text{C}$ and -65 to $-80\text{ }^{\circ}\text{C}$. In table 2, we report the number of cloud-top-surface pixels, those where $-CG$ and $+CG$ stroke densities are non null, and their percentages in each broad temperature bin. The number of GOES-8 pixels with non-null $-CG$ or $+CG$ stroke density is the greatest in the warmest temperature bin and decreases with CTT. 81%, respectively 80%, of the non-null $-CG$ stroke density pixels, respectively $+CG$, occur in thundercloud with CTT warmer than $-50\text{ }^{\circ}\text{C}$ and 97% of non-null $\pm CG$ stroke density pixels occur in thundercloud with CTT warmer than $-65\text{ }^{\circ}\text{C}$. These high percentages of non-null stroke densities associated with the warmest cloud top are due to the high percentage of thunderclouds with CTT belonging to the warmest broad temperature bins. Indeed, 99% of clouds observed by GOES-8 (not necessarily thunderclouds) have CTT warmer than $-65\text{ }^{\circ}\text{C}$. In the last two lines of table 2, the ratios of the number of pixels with a non-null stroke density to the number of available pixels in each broad temperature bins are given. These ratios increase

with decreasing CTT. About 10% of clouds with CTT between -10 and -35 °C produce -CGs ; this is 54% for clouds belonging to the coldest temperature bin. The proportion of clouds producing +CGs is about 5 times lower than those producing -CGs, whatever the CTT. However, this proportion increases with decreasing CTT, as for -CGs. Thus, the results reported in table 2 indicate that any positive or negative stroke density pixel is more likely associated with warmest CTT, but that clouds with coldest CTT are more likely to produce either kind of CGs.

A more detailed analysis of the stroke density distributions is shown in figure 4. In figure 4-a, the curves indicate the conditional probabilities that -CG stroke densities belong to any stroke density discretization bins, in each broad temperature bin. The curves of figure 4-b correspond to the same kinds of probabilities but for +CGs. The symbols plotted on curves indicate the middle of the stroke density discretization bins. The -CG probabilities are grossly similar for the different temperature bins (figure 4-a) . The percentage of pixels with stroke densities lower than $0.68 \text{ stroke km}^{-2} \text{ h}^{-1}$ varies from 70 to 84%, from the coldest to the warmest temperature bins. Thus, whatever the CTT, most stroke densities are lower than $0.68 \text{ stroke km}^{-2} \text{ h}^{-1}$. Each -CG probability curve displays a decrease with increasing stroke densities between 0.68 and $48 \text{ stroke km}^{-2} \text{ h}^{-1}$. In this stroke density range, the probabilities are similar for CTT between -10 and -65 °C and are two to five times higher in the coldest broad CTT bin. This trend does not continue for the cases of very high -CG stroke densities (greater than $48 \text{ stroke km}^{-2} \text{ h}^{-1}$). Thunderclouds with CTT ranging from -35 to -65 °C are apparently more likely producing these very high stroke density events than are thunderclouds with the coldest CTTs (between -65 and -80 °C).

Similar distributions for +CG stroke densities are plotted in figure 4-b in the four broad temperature bins. The curves of figure 4-b display a preferential stroke-density bin, whatever the CTT. Indeed, the probability that a cloud produces +CG densities between 0.108 and 0.18 *stroke km⁻² h⁻¹* is greater than 54% in any temperature bin. The grid size is variable in the study domain and varies from 10 × 10 *km²* at the lowest latitudes (30 °N) to 15 × 15 *km²* at the highest (55 °N). Thus, a stroke density of 0.14 *stroke km⁻² h⁻¹* corresponds to 14 *strokes/mesh/ h⁻¹* at the lowest latitude and to about 31.6 *strokes/mesh/ h⁻¹* at the highest latitudes. In the major part of the study domain the grid size is about 12 × 12 *km²* ; that is comparable to the dimension of single convective cells, and these results indicate that most convective cells have stroke densities roughly between 3.9 and 6.4 *strokes/convective cell/15min* or 0.2 and 0.4 *strokes/convective cell/min*. For stroke densities between 0.2 and 8 *stroke km⁻² h⁻¹*, the +CG probabilities decrease in all the four temperature bins. Unlike the -CG probabilities, the curve associated with the coldest temperature bin doesn't significantly differ from the others.

The convective vigor of storms is believed both to promote the cloud electrification and also to adjust the gap between the main negative charge center and the lower positive charge center, in terms of a thundercloud electrical structure is tripolar and is constituted by a upper positive, a main negative and a lower positive charge [MacGorman *et al.*, 1989]. By increasing the gap between the main negative charge center and the lower positive charge center, an increasing thundercloud updraft will first increase the -CG rate and finally for the strongest updrafts, will reduce the -CG rate, thus increasing thus the ratios +CG/-CG and IC:-CG. This non-linear effect is illustrated in the figure 1 of Lang

and Rutledge [2002] and is called the “charge-elevated mechanism”. Such a mechanism is consistent with statistics reported in figure 4.

The purpose of the next sections is to investigate two particular topics revealed in the current section. These topics are :

1. the increased probability of thunderstorms to produce at least one positive or one negative CG, as CTT decreases.
2. the behavior of CG density versus CTT

4. CTT and Probability of Cloud to Produce CGs

The results of table 2 show that the likelihood of lightning increases as CTT becomes colder. However, the decrease of CTT is observed on bulk CTT bins (15 °C wide) without regional and seasonal distinction. We analyse in the current section, the probability that a cloud-top-surface unit area at a given CTT be associated with positive or negative CGs. Cloud-top-surface area comparisons are chosen rather than pixel comparisons, because of the variable size of pixels. In order to show different mechanisms involved in the probability of a cloud-top-surface unit area to belong to a thundercloud producing at least one CG (hereafter called “CGP”), the regular CTT discretization bins defined in section 2.1 are used. Moreover, CGPs are detailed in each region defined in figure 1 and for each month from May to October 1999. CGP rates are given for the two polarities by :

$$\begin{aligned}
 \pm CGP(CTT, area, month) = & \frac{[cloud-top\ surface\ area\ where\ the\ \pm CG\ stroke\ density > 0](CTT, region, month)}{[total\ cloud-top\ surface\ area](CTT, region, month)} \\
 & (1)
 \end{aligned}$$

Figure 5-a, b, c, d and e shows $-CGP$ computed in May, June, July and August, September and October respectively. In each of these figures, the different curves represent $-CGP$ in a particular region. In May (graph a), all the curves display maxima at temperatures depending on regions of storm occurrences. CGPs increase for warmest CTT and display steeper slopes around -40 or -50 °C in regions 0, 1, 3 and 4 than in regions 2 and 5. In regions 0, 1, 3 and 4, the probabilities vary from low values (0.1-0.3) to high values (0.7-0.8) near -60 °C. In region 2 and 5, corresponding respectively to land regions near the Mexico Gulf and Florida, $-CGP$ is higher than in other regions, at CTT warmer than about -45 °C. In region 2, $-CGP$ doesn't display an obvious gradient. It ranges between 0.5 and 0.6 except for the coldest CTT, while by contrast a gradient is obvious in region 5 ranging from 0.4 at the warmest CTTs to 0.75 near -50 °C. The $-CGP$ features vary from month-to-month and from region-to-region. In October, only regions 0 and 3 display low $-CGP_s$ at warmest CTTs and experience a sharp increase to reach coldest CTT maxima. The other curves show multiple-peaks and a quasi-constant trend in region 4. In June, July-August and September, the features of May are partially reported. All the regions experience a $-CGP$ increase as CTT decreases. The high level maximum is seen only in regions 1 and 4, while existing in all regions in May. The sharp gradient occurs for regions 0, 3, 4 and 2 in July-August around -50 °C.

$+CGP$ are displayed in figure 6. $+CGP$ are low overall compared to $-CGP$. $+CGP$ maxima reach 0.4 while $-CGP$ maxima are about double. Nevertheless, the shapes of $+CGP$ and $-CGP$ curves are very similar. In May, $+CGP$ display maxima in all the regions. In May, June, July-August and September all the regions show a gross increase of $+CGP$ with decreasing CTT. Regions 0, 3 and 4 show a steep slope of $+CGP$ around

-40 or -50 °C in any month and a steep slope is also displayed in July-August for region

2. This has been also observed for $-CGP$.

Several parameters can affect the $\pm CGP$ profiles. The “total cloud surface” used in the denominator of equation 1 can include both storm and non storm-related clouds. Moreover, CTT can also be a factor determining CGP because it is related to the convective vigor of clouds. It is shown in section ??, by comparing overall stroke densities and restricted overall stroke densities, that the influence of non-stormy clouds is significant for CTT warmer than about -50 °C. For CTT colder than -50 °C, an increase of CGP is observed as CTT decreases. This increase can be due to a correlation between the cloud-electrification efficiency and the convective vigor. However, as CTT decreases the $-CGP$ profiles reach a maximum, and decrease at highest level in May for all regions and in any month for region 4. That is consistent with the charge-elevated mechanism. If this is actually the mechanism implied in the $-CGP$ profiles, then questions arise : Why is this mechanism prevailing only in May 1999 for all the regions, and any time over the mountainous region (region 4) ? Moreover, $+CGP$ displays the same high level maxima as $-CGP$; this is not consistent with the charge-elevated mechanism, except if the thunderclouds involved in the maxima feature inverted-dipole charge distributions [Seimon, 1993].

Relationships showing the lightning probability increase with cloud-top height have already been observed by *Holle and Maier* [1982]. The results of *Dye et al.* [1989] concerning New Mexico storms show a similar trend. They sampled 20 electrified storms, among which 6 never produced lightning. These 6 clouds had the lowest cloud-top height (between 8 and 9.5 km). The other clouds, all of which produced lightning, exhibited

cloud tops higher than 10 km, except one of 9 km height. Less frequent are studies concerning the lack of CGs in very deep continental storms as CGP sometimes suggests. That is shown for deep storms occurring over the tropics [Rutledge *et al.*, 1992; Rutledge and Petersen, 1994; Zipser, 1994] but the particular meteorological conditions met in the tropics are certainly not operative in the continental United States. Lang *et al.* [2000], Lang and Rutledge [2002] reported storms with anomalously low -CG flash rate and high +CG flash rate, for which they invoked the charge-elevated mechanism. Decrease of $\pm CGP$ associated with coldest CTT can also be attributable to the ground-flash-polarity switch observed during severe weather [MacGorman and Burgess, 1994; Perez *et al.*, 1997].

4.1. CTT and Overall Stroke Density

Another insight can be gained if we take into account the intensity of the CG activity.

This is done by computing a kind of overall stroke density as follow :

$$GSD(CCT, region, month) = \frac{(\# \text{ of strokes}(CTT, region, month))}{(total \text{ thundercloud} - top \text{ surface area})(CTT, region, month)} \quad (2)$$

where the number of strokes is integrated over 15-minute epochs and converted to a number of strokes per hour and, the total thundercloud-top-surface area is expressed in km^{-2} . A thundercloud-top-surface is defined as a cloud-top-surface where at least one positive or negative CG is detected. GSD is tallied each month and region, for +CGs (called $+GSD$) and for -CGs (called $-GSD$) (figure 7 and 8 respectively) . In graphs a, b, c, d and e of figure 7 and 8, the curves represent $-GSD$ in each regions and the graphs are for May, June, July-August, September and October respectively.

Monthly and regional profiles of $+GSD$ are plotted in figure 8 similarly to $-GSD$. $+GSD$ is about 1 order of magnitude lower than $-GSD$. Despite the magnitude differ-

ence, the profiles of $+GSD$ exhibit the same kind of shapes than $-GSD$. $\pm GSD$ profiles are quasi-vertical for CTT between -10 and -55 °C (sometimes colder). Increases of $\pm GSD$ are usually obvious for CTT colder than -55 °C, but sometimes, $\pm GSD$ decreases at the coldest CTT. This is consistent with the “charge-elevated mechanism”. We note also that $\pm GSD$ are grossly higher in regions of lower latitude.

Let us look by another way at the overall stroke densities. The number of strokes produced per hour in a CTT bin (see section 2.1), and the overall cloud-top-surface area where the CG densities of the corresponding polarity are greater than zero, are now consider. The values of these two parameters are plotted in figure 9 for -CGs and 10 for +CGs. Each data point is for a regular temperature bin.

These results show that CG-thunderstorms of a given region and month produce a quasi constant stroke density. Results of region 1 in May for both positive and negative CGs (figure 9-a and 10-a) are not aligned and are related to a low number of statistical events. It is shown earlier that the major differences between straight-line fits are not their slopes but their intercepts. Thus, the major difference from region-to-region between straight-line fits can be related to the value of the cloud-top-surface areas for which the number of strokes is null. These cloud-top-surface areas can be seen as threshold areas that a thunderstorm-top-surface must reach to produce CGs. Once a thunderstorm has reached this threshold area, that is region and month dependent, a given cloud-top-surface area anywhere in the CONUS produces roughly the same number of lightning per unit area (grossly similar slope of straight lines). Thus, these results show that the CG stroke density is, in a first approximation, neither month nor regional dependent.

In order to analyse more accurately the relationships between the number of strokes and the cloud-top-surface areas, quadratic polynomial fits have been computed to data of figures 9 and 10. Because the second order coefficients are always at least 10^{-6} times less than the first order coefficients, the second order coefficients are not reported in table 3. Thus, the equations leading to the number of positive and negative strokes from a given CG-thundercloud-top-surface area are linear and expressed as : $NS = a + b \times S$, where NS is the number of stroke produced per hour, S is the cloud-top-surface area (km^2), a is the intercept parameter ($stroke\ h^{-1}$) and b is the slope parameter that has the dimension of a stroke density ($stroke\ km^{-2}\ h^{-1}$). The values of the intercept parameters are of about 10^4 or 10^5 for -CGs and of an order of magnitude less for +CGs. The intercept parameter values vary a lot from region-to-region in May 99 whatever the CG polarity but are relatively close from month-to-month. Let us analyse the surface areas corresponding to a null stroke density (threshold surface areas). As discussed above, it is obvious from figures 9 and 10 that the threshold surface areas are region dependent and are higher in regions of lower latitude (this is confirmed by numerical values of table 3). Nevertheless, these threshold surface areas, which are the ratio $\frac{-a}{b}$ (table 3), are sometimes negative (i.e. without meaning). Certainly because the range of validity of the linear fits is limited. The slope coefficients for $\pm CGs$ displayed in table 3 are also plotted in figure 11 for the different regions and month of the study. As the intercept parameters, the slope coefficients are dispersed in May 99 and are also closer from one region to another the other months from June to October. The slope parameters are around $0.04\ stroke\ km^{-2}\ h^{-1}$ for -CGs and around $0.02\ stroke\ km^{-2}\ h^{-1}$. The slopes vary more widely from region-to-region than from month-to-month. Moreover, as the number of strokes produced by a given

CG-thundercloud-top-surface area (figures 9 and 10), the slope parameters are ranked according to the central latitude of their related region. The slope parameters are higher in regions of lower latitude. Figures 9 and 10 show that the number of positive or negative CGs are more numerous for a given thundercloud-top-surface area at low latitude than for the same surface at higher latitude, moreover figure 11 shows that an increase in the CG-thundercloud-surface area will increase the associated number of CGs more if the thunderstorm occurs at lower latitude.

5. Discussion

In this study, CTT appear to be correlated to CTT. This is consistent with current knowledge on relation between convective vigor of clouds and lightning flash rates. Higher the convective vigor of cloud, higher is the rate of cloud electrification and thus higher is the probability for a cloud to produce lightning and specifically CGs, except for the tallest cloud affected by the charge-elevated mechanism (also consistent with the current results).

Extrapolations of the point pairs corresponding to the number of CGs of a given polarity and the associated cloud-top-surface area with CTT comprised in regular temperature bin, indicate a possible role of threshold cloud-top-surface areas, above which one or more CG are produced. These threshold surface areas decrease as the storm latitude decreases. In regions of higher latitude, where the cloud vertical development is lower, higher cloud surface areas are necessary for clouds to become CG-thunderclouds. This is consistent with *Williams* [2001] who wrote “laterally extensive charge regions are more likely to provide the electrostatic energy necessary to bridge the long gap to ground”.

The behavior of clouds with CTT colder than $-55\text{ }^{\circ}\text{C}$ (20 % of the cloud-top surfaces associated with non null CG densities) is consistent with the positive correlations between convective vigor of clouds and lightning flash rate reported in some studies that are at the origin of scaling laws : *Vonnegut* [1963]; *Cherna and Stansbury* [1986]; *Price and Rind* [1992]; *Williams* [1985, 2001].

Most of the events, at least 70%, have close stroke densities (less than $0.68\text{ Stroke km}^{-2}\text{h}^{-1}$ for -CGs and between 0.108 and $0.18\text{ Stroke km}^{-2}\text{h}^{-1}$) whatever CTT. Moreover, for more than 80% of the events with CTT warmer than $-55\text{ }^{\circ}\text{C}$, *GSDs* are very close whatever CTT if they belong to the same region. These observations suggest that most of CG thunderclouds have quasi-constant stroke density. This is confirmed by figures 9, 10 and 11 and the linear CG-number per time unit/CG-thundercloud-top-surface area relationships. These relationships also indicate that the parameter the most determining the quasi-constant stroke density is the latitude of storm occurrence. Different hypothesis are proposed for the CG-density insensitivity to CTT :

1. CTT is not a good indicator of the convective state of thunderclouds and therefore, in most of the cases, no relationships can be expected between CTT and CG densities. It is difficult to give definitive conclusions on this issue because few or none comparative studies on thundercloud top heights measured from space at $10.7\text{ }\mu\text{m}$, and radar reflectivities, several times related to the cloud electrical level, or other meteorological parameters indicating the thundercloud convective vigor, were published.

2. If CTT is a convenient indicator of the thundercloud convective vigor, therefore, quasi-constant CG densities associated with any CTT ranging from -10 to $-55\text{ }^{\circ}\text{C}$, indicate

that other mechanisms than CGs release the electrical-stress swell up, owed to increase thundercloud convective vigors leading CTT from -10 to -55 °C. One of these mechanisms can be the IC lightning flashes. It has already been reported that the IC likelihood increases as the storm convective vigor [*Rutledge et al.*, 1992; *Lang and Rutledge*, 2002]. On the same way, *Rutledge et al.* [1992] (for tropical clouds) and *Chèze and Sauvageot* [1997] (for continental clouds) reported increases of the IC:CG ratio as the total flash rate. If the CG stroke density is actually constant whatever CTT comprised between -10 and -55 °C, the relationship given by *Chèze and Sauvageot* [1997] becomes particularly useful because in this case, the IC rate measurement is sufficient to determine the total flash rate.

3. CTT is a convenient indicator of only some cloud stages. *Liu and Curry* [1998] compared IWP, LWP (liquid water path that is the column integrated liquid water content) and CTT in tropical clouds. They found IWP and LWP well correlated if CTT is colder than -40 °C. They found also good correlation between CTT and IWP although CTT doesn't allow to distinguish between heavy precipitating and non or high-precipitating clouds. In our case, this is done by selecting CG thunderstorms known to be associated with precipitating clouds (see *Molinié et al.* [1999] for example). As liquid and ice water are both required to involve cloud electrification, we can expect a correlation between CTT and CG densities for clouds with CTT higher than -40 °C. This is found for CTT colder than about -55 °C. However, for CTT warmer than -40 °C, although CTT and IWP remain well correlated, *Liu and Curry* [1998] noted that IWP and LWP are decoupled. Thus, a CTT decrease implies IWP increases but not necessarily LWP increases. In this case, it can be more difficult to observe correlations between CTT and CG densities.

However, *Koffi N'Dri et al.* [2000] succeed using GOES-8 channel 4 and Meteosat infrared data to follow the early development of convective clouds. Therefore, the misidentification of cloud electrical vigor via CTT would concern mature and decaying stage of thunderstorms with CTT warmer than $-55\text{ }^{\circ}\text{C}$. Moreover, it has been shown in several studies [*Goodman et al.*, 1988; *Williams et al.*, 1989; *Williams*, 1985; *Carey and Rutledge*, 1998] that most of the CGs in most of the storms occur during the mature and the decaying stage of thundercloud. This consistent with the CG-density insensitivity to CTT for CTT warmer than about $-55\text{ }^{\circ}\text{C}$ observed in the current work and that concern the major part of studied events.

Beside the quasi-independence of the $\pm CG$ density to CTT, we must consider the strong dependence of the $\pm CG$ density to the latitudes of thunderstorm-occurrences while the thunderstorm longitudes are insensitives. Zonal averages of the tropopause height are strongly dependent of the latitude. It decreases from about 16 km at the equator to 10 km at $40\text{ }^{\circ}\text{North}$. It is well known that the tropopause height leads the thundercloud-top maximum development that is reached at the mature stage. The occurrence of most of CGs during the mature or decaying stage of thunderclouds is consistent with the CG-density strong dependence to the thundercloud latitude. Under this assumption, for most of the clouds ($\text{CTT} > -55\text{ }^{\circ}\text{C}$) the tropopause height and in a statistical sense the latitude of storms occurrence are better indentifications of the thunderstorm height than CTT. Thus, the correlation between CGdensities and latitude can be seen as an illustration of scaling laws assuming a correlation of thunderstorm height and electrical activity level.

6. Conclusions

In this study, we use CTT data issued from GOES-8 channel 4 ($10.7\mu m$) measurements and NLDN data to compute lightning stroke densities. These data are compared in 5 different geographical regions covering the CONUS from May to October 1999.

We have shown that the majority of CGs are associated with low cloud top and low stroke densities. It is also shown that no preferential CTT are associated with high -CG or +CG stroke densities.

The likelihood of a cloud to become a CG thundercloud increases as CTT decreases. We also infer that a threshold cloud-top-surface area is required for clouds to become CG-thunderclouds. This threshold cloud-top-surface area increases with the latitude of storm occurrence.

CG densities are found increasing as CTT decrease only in cloud with CTT colder than about $-55\text{ deg }C$. That comprises only 20% of clouds. For the majority of clouds (for which CTT is warmer than $-55\text{ }^{\circ}C$) no relation is observed between CTT and CG densities. Moreover, CG densities are quasi-constant whatever CTT. Thus, regional scaling relations are given linking CG thundercloud-top-surface areas and $\pm CG$ densities.

CG densities are found to be strongly correlated to the latitude of storm occurrences. This is likely related to the tropopause height.

Acknowledgments. (text here)

References

Carey, L. D., and S. A. Rutledge, A multiparameter radar case study of the microphysical and kinematic evolution of a lightning producing storm, *Meteorology and Atmospheric*

Physics, 59, 33–64, 1996.

Carey, L. D., and S. A. Rutledge, Electrical and multiparameter radar observations of a severe hailstorm, *J. Geoph. Res.*, 103, 13,979–14,000, 1998.

Cherna, E. V., and E. J. Stansbury, Sferics rate in relation to thunderstorm dimensions, *J. Geoph. Res.*, 91, 8701–8707, 1986.

Chèze, J. L., and H. Sauvageot, Area-average rainfall and lightning activity, *J. Geoph. Res.*, 102, 1707–1716, 1997.

Cummins, K. L., M. J. Murphy, E. A. Bardo, W. L. Hiscox, R. B. Pyle, and A. E. Pifer, A combined toa/mdf technology upgrade of the us national lightning detection network, *J. Geoph. Res.*, 103, 9035–9044, 1998.

Dye, J., J. Jones, W. Winn, T. Cerni, B. Gardiner, D. Lamb, R. Pitter, J. Hallet, and C. Saunders, Early electrification and precipitation development in a small, isolated montana cumulonimbus, *J. Geoph. Res.*, 91, 1231–1247, 1986.

Dye, J., W. Winn, J. Jones, and D. Breed, The electrification of new mexico thunderstorms 1. relationship between precipitation development and the onset of electrification, *J. Geoph. Res.*, 94, 8643–8656, 1989.

Fister, V., H. von Rheinbaben, and T. Zundl, Analyses of the 1992 and 1993 lightning data in south germany, in *22 nd. Int. Conf. Lightning Protection*, Preprints, pp. 211–216.

Gardiner, B., D. Lamb, L. Pitter, R., and J. Hallet, Measurements of initial potential gradient and particle charges in a montana summer thunderstorm, *J. Geoph. Res.*, 90, 6079–6086, 1985.

Goodman, S. J., D. E. Buechler, and P. D. Wright, Lightning and precipitation history of a microburst-producing storm, *Geoph. Res. Let.*, 15, 1185–1188, 1988.

- Holle, R. L., and M. W. Maier, Radar echo height related to cloud to ground lightning in south florida, *Preprints, 12 th Conf. on Severe Local Storms, American Meteorological Society*, 1982.
- Huffines, G. R., and R. E. Orville, Lightning ground flash density and thunderstorm duration in the continental united states: 1989-96, *J. Appl. Meteor.*, *38*, 1013–1019, 1999.
- Idone, V. P., D. A. Davis, P. K. Moore, Y. Wang, R. W. Henderson, M. Ries, and P. F. Jamason, Performance evaluation of the u.s. national lightning detection network in eastern new york. part ii : location accuracy, *J. Geoph. Res.*, *103*, 9045–9055, 1998.
- Jayaratne, E., C. Saunders, and J. Hallet, Laboratory studies of the charging of soft-hail during ice crystal interactions, *Quart. J. Roy. Meteor. Soc.*, *109*, 609–630, 1983.
- Johnson, D., P. Flament, and R. Bernstein, High-resolution satellite imagery for mesoscale meteorological studies, *Bull. Am. Meteor. Soc.*, *75*, 5–33, 1994.
- Kane, R., Correlating lightning to severe local storms in the northeastern united states, *Weather and Forecasting*, *6*, 3–12, 1991.
- Koffi N'Dri, E., S. Senesi, and C. Morel, Early convective development study using combined satellite and lightning data, *report to Eumetsat*, 2000.
- Lang, T. J., and S. A. Rutledge, Relationships between convective storm kinematics, precipitation, and lightning, *Mon. Wea. Rev.*, *130*, 2492–2506, 2002.
- Lang, T. J., S. A. Rutledge, J. Dye, M. Venticinque, P. Laroche, and E. Defer, Anomalous low negative cloud-to-ground lightning flash rates in intense convective storms observed during sterao-a, *Mon. Wea. Rev.*, *128*, 160–173, 2000.

- Liu, G., and J. A. Curry, Remote sensing of ice water characteristics in tropical clouds using aircraft microwave measurements, *J. Appl. Meteor.*, *37*, 337–355, 1998.
- MacGorman, D., and D. Burgess, Positive cloud-to-ground lightning in tornadic storms and hailstorms, *Mon. Wea. Rev.*, *122*, 1671–1697, 1994.
- MacGorman, D., D. W. Burgess, V. Mazur, R. W. D., W. L. Taylor, and B. C. Johnson, Lightning rates relative to tornadic storm evolution on 22 may 1981, *J. Atmos. Sci.*, *46*, 221–250, 1989.
- MacGorman, D. R., and W. D. Rust, *The electrical nature of storms*, at Oxford Univ. Pres, 1998, pp. 422.
- Molinié, G., S. Soula, and S. Chauzy, Cloud-to-ground lightning activity and radar observations of storms in the pyrénées range area, *Quart. J. Roy. Meteor. Soc.*, *125*, 3103–3122, 1999.
- Orville, R. E., Lightning ground flash desity in the contiguous united states – 1989, *Mon. Wea. Rev.*, *119*, 573–577, 1991.
- Orville, R. E., Cloud-to-ground lightning flash characteristics in the contiguous united states : 1989-1991, *J. Geoph. Res.*, *99*, 1994.
- Orville, R. E., and A. C. Silver, Lightning ground flash desity in the contiguous united states: 1992–95, *Mon. Wea. Rev.*, *125*, 631–638, 1997.
- Orville, R. E., G. R. Huffines, W. R. Burrows, R. L. Holle, and K. L. Cummins, The north american lightning detection network (naldn) : First results: 1998-2000, *Mon. Wea. Rev.*, *130*, 2098–2109, 2002.
- Parker, M. D., S. A. Rutledge, and R. H. Johnson, Cloud-to-ground lightning in linear mesoscale convective systems, *Mon. Wea. Rev.*, *129*, 1232–1242, 2001.

- Perez, A., L. J. Wicker, and R. E. Orville, Characteristics of cloud-to-ground lightning associated with violent tornadoes, *Weather and Forecasting*, *12*, 428–437, 1997.
- Price, C., and D. Rind, A simple lightning parameterization for calculating global lightning distributions, *J. Geophys. Res.*, *97*, 9919–9933, 1992.
- Price, C., J. Penner, and M. Prather, Nox from lightning, 1. global distribution based on lightning physics, *J. Geophys. Res.*, *102*, 5929–5941, 1997.
- Rubinstein, M., E. Montandon, and M. Ianoz, Analyses of multistation cloud lightning electric field pulses recorded with the swiss lpats network, in *22 nd. Int. Conf. Lightning Protection*, Preprints, p. 5 pp.
- Rutledge, S., and W. Petersen, Vertical radar reflectivity structure and cloud-to-ground lightning in the stratiform region of mcss: Further evidence for in situ charging in the stratiform region, *Mon. Wea. Rev.*, *122*, 1760–1776, 1994.
- Rutledge, S., E. Williams, and T. Kennan, The down under doppler and electricity experiment (dundee): Overview and preliminary results, *Bull. Am. Meteor. Soc.*, *73*, 3–16, 1992.
- Rutledge, S. a., and D. R. MacGorman, Cloud-to-ground lightning activity in the 10-11 june 1985 mesoscale convective system observed during the oklahoma kansas pre-storm project., *Mon. Wea. Rev.*, *116*, 1393–1408, 1988.
- Seimon, A., Anomalous cloud-to-ground lightning in an f5-tornado-producing supercell thunderstorm on 28 august 1990, *Bull. Am. Meteor. Soc.*, *74*, 189–204, 1993.
- Sheu, R., J. Curry, and G. Liu, Vertical stratification of tropical cloud properties as determined from satellite, *J. Geophys. Res.*, *102*, 4231–4245, 1997.

- Stolzenburg, M., Characteristics of the bipolar pattern of lightning locations observed in 1988 thunderstorms, *Bull. Am. Meteor. Soc.*, *71*, 1331–1338, 1990.
- Takahashi, T., Riming electrification as a charge generation mechanism in thunderstorms, *J. Atmos. Sci.*, *35*, 1536–1548, 1978.
- Tourte, J., F. Helloco, M. Le Boulch, and J. Hamelin, First results obtained with the météorage thunderstorm monitoring system, in *Proceedings of the 8th Conference on Atmospheric Electricity*, pp. 697–702, Institute of High Voltage Research, Uppsala University, 1988.
- Ushio, T., S. Heckman, D. Boccippio, H. Christian, and Z. Kawasaki, A survey of thunderstorm flash rates compared to cloud top height using trmm satellite data, *J. Geoph. Res.*, *106*, 24,089–24,095, 2001.
- Vonnegut, B., Some facts and speculations concerning the origin and role of thunderstorm electricity, *Severe Local Storms, Meteor. Monogr.*, pp. 224–241, 1963.
- Weinheimer, A., J. Dye, D. Breed, M. Spowart, J. Parrish, T. Hoglin, and T. Marshall, Simultaneous measurements of the charge, size, and shape of hydrometeors in an electrified cloud, *J. Geoph. Res.*, *96*, 20,809–20,829, 1991.
- Williams, E., B. Boldi, A. Matlin, M. Weber, S. Hodanish, D. Sharp, and S. Goodman, The behavior of total lightning activity in severe florida thunderstorms, *J. Atmos. Res.*, *51*, 245–265, 1999.
- Williams, E. R., Large scale charge separation in thunderclouds, *J. Geoph. Res.*, *90*, 6013–6025, 1985.
- Williams, E. R., *Meteorological monographs*, vol. 28, chap. 13 : The electrification of severe storms, pp. 527–561, American Meteorological Society, 2001.

Williams, E. R., M. Weber, and R. Orville, The relationship between lightning type and convective state of thunderclouds, *J. Geophys. Res.*, *94*, 13,213–13,220, 1989.

Zajac, B. A., and S. A. Rutledge, Cloud-to-ground lightning activity in the contiguous united states from 1995 to 1999, *Mon. Wea. Rev.*, *129*, 999–1019, 2001.

Zipser, E., Deep cumulonimbus cloud systems in the tropics with and without lightning, *Mon. Wea. Rev.*, *122*, 1837–1851, 1994.

Figure 1. Definition of the geographic regions where CTT/stroke density correspondences are computed. In these regions, the NDLN detection efficiency is at least 80 %.

Figure 2. a : Number of -CG stroke-density pixels available as a function of temperature in May 1999. b : same for June 1999 ; c : same for July-August 1999 ; d : same for September 1999 ; e : same for October 1999 ; keys : regional identification of curves .

Figure 3. same as figure 2 but for +CGs. Note change in horizontal scale relative to figure 2.

Figure 4. a: Probability of -CG densities to be co-located with CTT in temperature bins. b : same for +CGs.

Figure 5. *CGP* : ratio of the cloud-top-surface area that is in the high-resolution regular temperature bins where the -CG stroke density is non null, to the cloud-top-surface area available in the same temperature bins. Each curve corresponds to a different region (see key). Each graph is for a different month. a : May ; b : June ; c : July-August ; d : September ; e : October ; key : regional identification of curves.

Figure 6. same as figure 5 for +CG

Figure 7. *GSD* : ratio of the number of -CG strokes to the total cloud-top surface where any kind of CG density is non null, observed in the regular temperature bins. Each curve corresponds to a different region (see key). Each graph is for a different month. a : May ; b : June ; c : July-August ; d : September ; e : October ; key : Regional identification of curves.

Figure 8. same as figure 7 for +CG

Figure 9. Point pairs ($\#$ -CG strokes, CG thundercloud-top-surface area where the -CG density is non null). Each graph is for a different month. a : May ; b : June ; c : July-August ; d : September ; e : October ; key : regionnal affiliation of curves

Figure 10. same as figure 9 for +CG

Figure 11. Slope coefficients and intercepting values for linear regressions of the number of lightning produced by a given cloud-top-surface. Slope coefficients plotted in graphs a and b are in *stroke km⁻² h⁻¹* and correspond respectively to -CGs and +CGs.

Table 1. Number of events in each stroke or flash category used in this statistical study.

	May	June	July	August	September	October
+CG	1,911,955	3,278,871	1,569,209	3,060,319	2,614,651	766,920
-CG	5,974,982	14,022,062	5,394,138	16,063,690	14,554,957	2,655,192

Table 2. In each broad temperature bin, the number of non-null $\pm CG$ density pixels, GOES-8 pixels and the percentage of each of these pixels regarding their number in all the temperature layers are given. In the last two lines, the ratio of the number of non-null -CG and +CG stroke density pixels to the number of GOES-8 pixels are shown.

Temperature bins	$-20 > T > -35$ <i>C</i>	$-35 > T > -50$ <i>C</i>	$-50 > T > -65$ <i>C</i>	$-65 > T > -80$ <i>C</i>
-CG	13,563,333	9,881,195	4,518,166	694,261
% -CG	47	34	16	3
+CG	3,019,676	2,201,073	1,112,888	191,185
% +CG	46	34	17	3
GOES-8	115,640,192	66,850,200	15,780,512	1,275,841
% GOES-8	58	33	8	1
-CG/GOES-8	0.11	0.14	0.26	0.54
+CG/GOES-8	0.02	0.03	0.07	0.14

Table 3. Relationship giving the number of \pm CG strokes per hour and per cloud-top-surface area S (km^2) where at least one \pm CG were detected in a 15 min epoch. Each month, the first line corresponds to -CGs and the second one to +CGs.

DATE	REGION 0	REGION 1	REGION 2
199905	$9.68.10^5 + 5.05.10^{-2} \times S$ $6.31.10^4 + 2.20.10^{-2} \times S$	$5.13.10^2 + 1.34.10^{-2} \times S$ $3.89.10^2 - 1.24.10^{-1} \times S$	$8.28.10^4 + 9.85.10^{-2} \times S$ $-1.07.10^4 + 4.25.10^{-2} \times S$
199906	$-1.37.10^4 + 4.25.10^{-2} \times S$ $8.44.10^1 + 1.30.10^{-2} \times S$	$-2.72.10^2 + 1.28.10^{-2} \times S$ $1.37 + 5.46.10^{-3} \times S$	$8.13.10^4 + 6.37.10^{-2} \times S$ $3.92.10^2 + 2.18.10^{-2} \times S$
199907	$4.25.10^5 + 4.00.10^{-2} \times S$ $5.64.10^3 + 1.33.10^{-2} \times S$	$3.36.10^2 + 2.28.10^{-2} \times S$ $-6.79.10^2 + 6.92.10^{-3} \times S$	$1.86.10^4 + 5.02.10^{-2} \times S$ $5.67.10^2 + 1.83.10^{-2} \times S$
199908	$7.85.10^5 + 3.56.10^{-2} \times S$ $1.20.10^4 + 1.24.10^{-2} \times S$	$4.29.10^4 + 2.41.10^{-2} \times S$ $2.25.10^3 + 6.93.10^{-3} \times S$	$1.72.10^5 + 6.93.10^{-2} \times S$ $5.61.10^3 + 2.01.10^{-2} \times S$
199909	$1.29.10^5 + 3.82.10^{-2} \times S$ $4.66.10^3 + 1.19.10^{-2} \times S$	$4.40.10^2 + 8.25.10^{-3} \times S$ $4.57.10^2 + 3.87.10^{-3} \times S$	$4.86.10^4 + 6.76.10^{-2} \times S$ $3.41.10^3 + 1.86.10^{-2} \times S$
199910	$4.78.10^4 + 3.21.10^{-2} \times S$ $-1.92.10^3 + 1.17.10^{-2} \times S$	$3.73.10^2 + 6.85.10^{-3} \times S$ $3.42.10^2 + 5.55.10^{-3} \times S$	$2.71.10^4 + 5.72.10^{-2} \times S$ $2.07.10^2 + 1.88.10^{-2} \times S$
DATE	REGION 3	REGION 4	REGION 5
199905	$3.80.10^5 + 4.41.10^{-2} \times S$ $3.44.10^4 + 2.00.10^{-2} \times S$	$3.05.10^5 + 4.35.10^{-2} \times S$ $2.46.10^4 + 1.78.10^{-2} \times S$	$3.00.10^4 + 1.47.10^{-1} \times S$ $2.95.10^3 + 4.74.10^{-2} \times S$
199906	$-2.15.10^5 + 5.00.10^{-2} \times S$ $-5.35.10^3 + 1.32.10^{-2} \times S$	$3.97.10^2 + 3.53.10^{-2} \times S$ $9.35.10^2 + 1.27.10^{-2} \times S$	$3.32.10^4 + 8.27.10^{-2} \times S$ $2.62.10^3 + 2.80.10^{-2} \times S$
199907	$3.35.10^5 + 3.92.10^{-2} \times S$ $9.57.10^3 + 1.30.10^{-2} \times S$	$7.04.10^4 + 3.95.10^{-2} \times S$ $-9.56.10^2 + 1.36.10^{-2} \times S$	$1.42.10^4 + 8.05.10^{-2} \times S$ $3.77.10^2 + 2.58.10^{-2} \times S$
199908	$6.75.10^4 + 3.79.10^{-2} \times S$ $6.07.10^3 + 1.18.10^{-2} \times S$	$2.06.10^5 + 3.24.10^{-2} \times S$ $3.66.10^1 + 1.25.10^{-2} \times S$	$1.36.10^5 + 8.59.10^{-2} \times S$ $2.22.10^3 + 2.64.10^{-2} \times S$
199909	$-1.03.10^5 + 4.34.10^{-2} \times S$ $-3.59.10^2 + 1.21.10^{-2} \times S$	$1.29.10^5 + 3.16.10^{-2} \times S$ $-1.68.10^3 + 1.18.10^{-2} \times S$	$6.68.10^4 + 7.86.10^{-2} \times S$ $3.96.10^2 + 2.93.10^{-2} \times S$
199910	$2.61.10^3 + 3.28.10^{-2} \times S$ $-2.33.10^3 + 1.18.10^{-2} \times S$	$4.58.10^2 + 1.89.10^{-2} \times S$ $2.16.10^2 + 1.12.10^{-2} \times S$	$-2.56.10^3 + 7.00.10^{-2} \times S$ $-9.41.10^1 + 2.72.10^{-2} \times S$

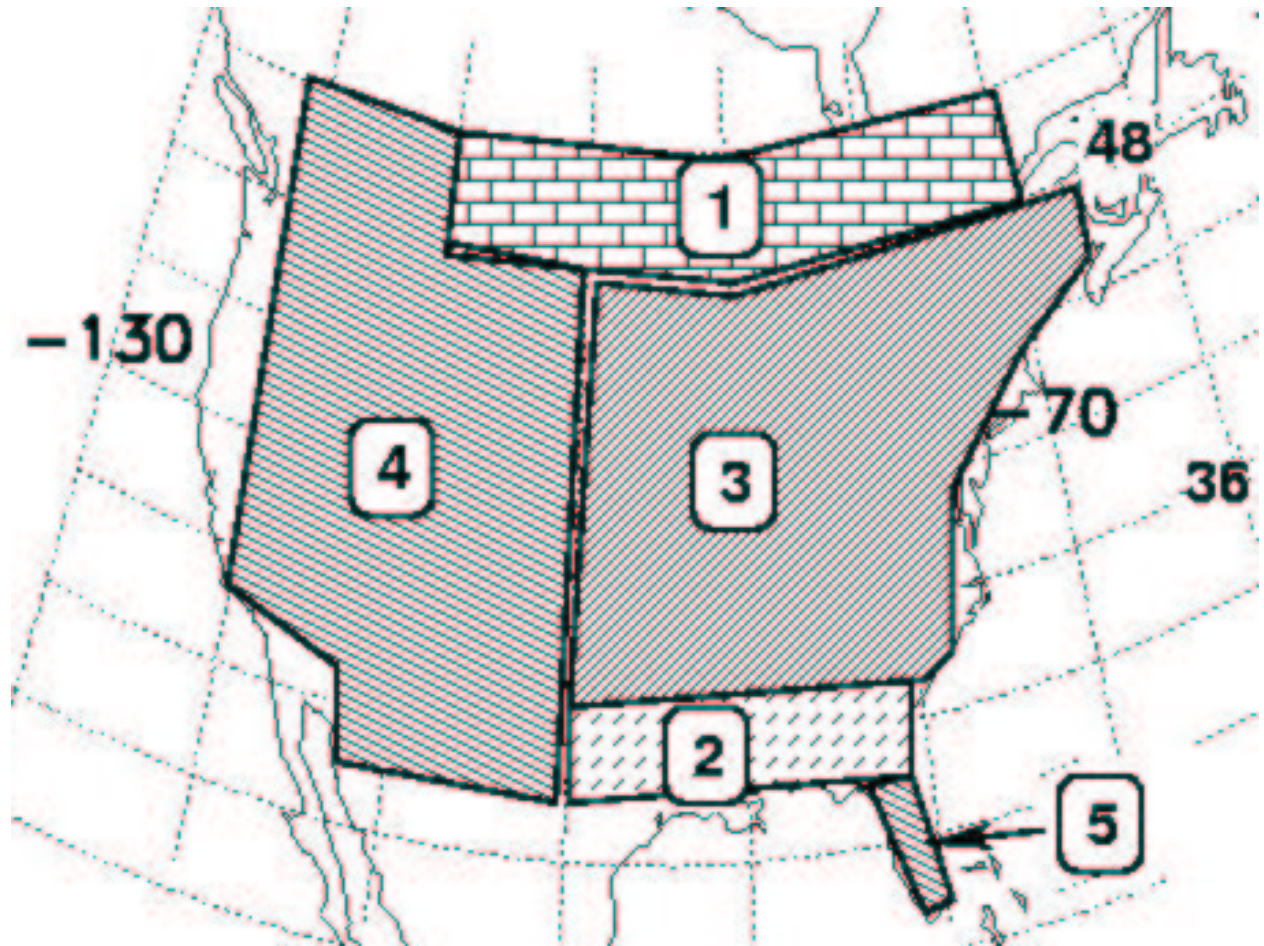


Figure 1: Definition of the geographic regions where CTT/stroke density correspondances are computed. In these regions, the NDLN detection efficiency is at least 90 %.

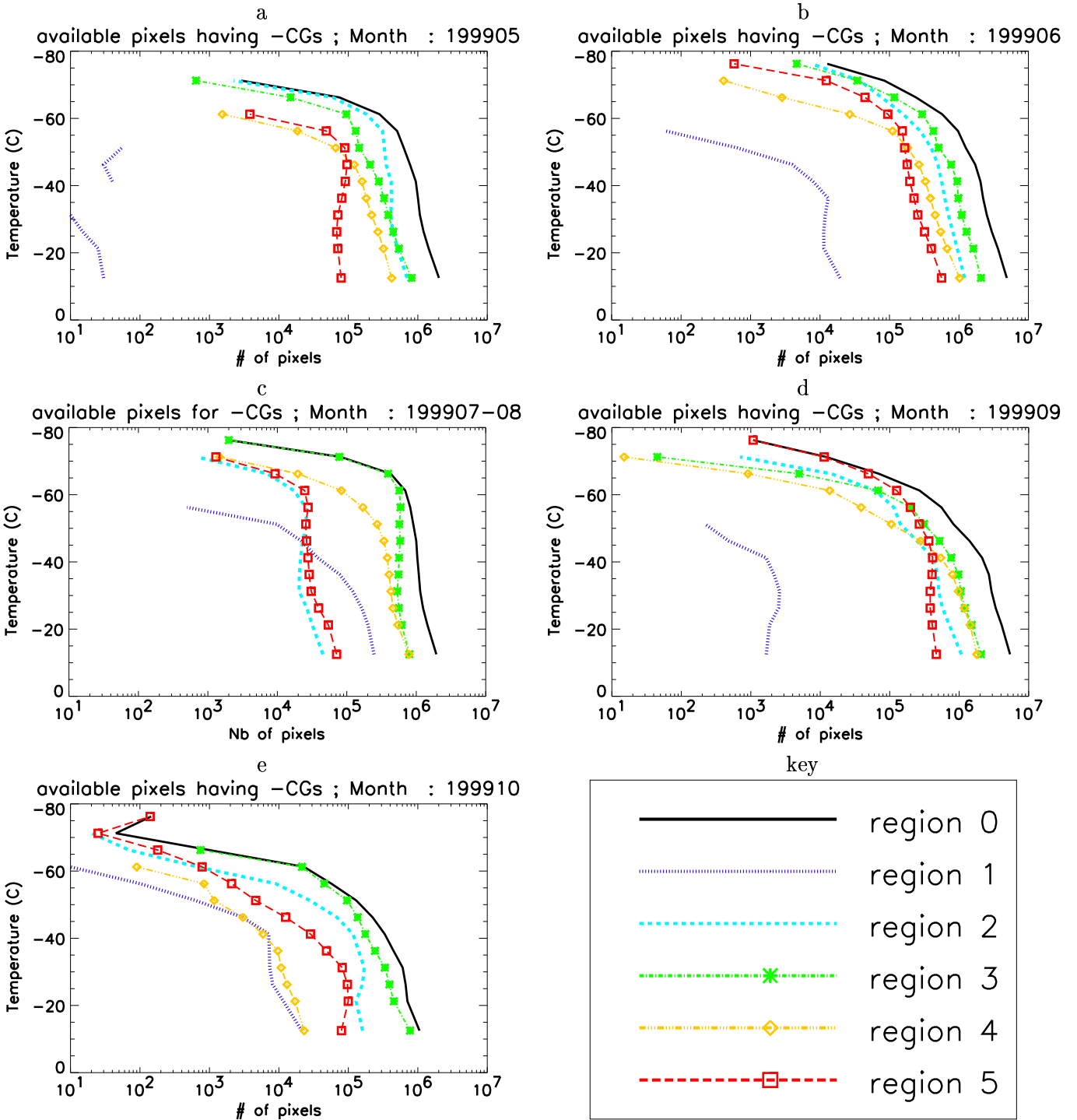


Figure 2: a : Number of -CG stroke-density pixels available as a function of temperature in May 1999. b : same for June 1999 ; c : same for July-August 1999 ; d : same for September 1999 ; e : same for October 1999 ; key : regional identification of curves .

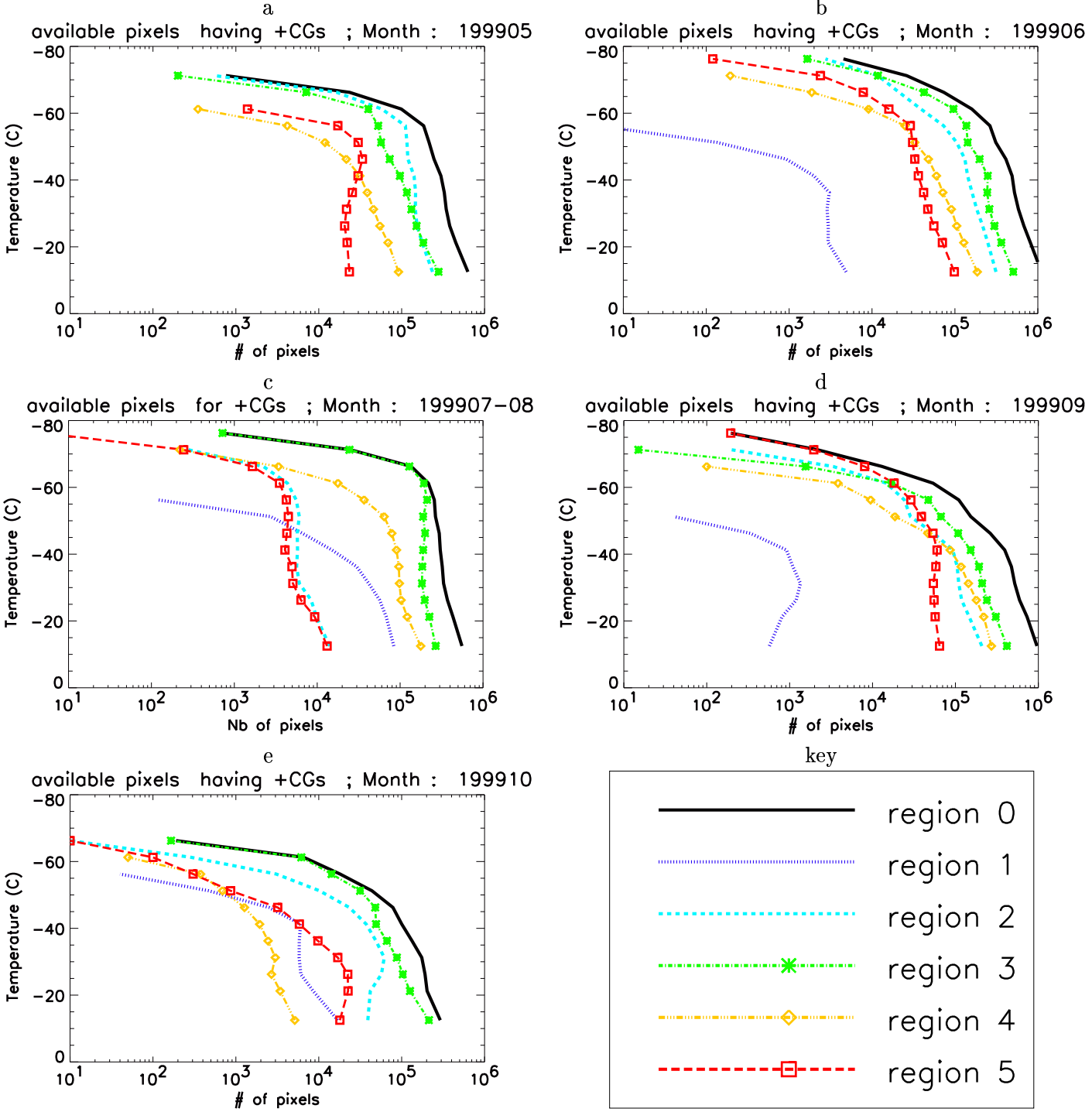
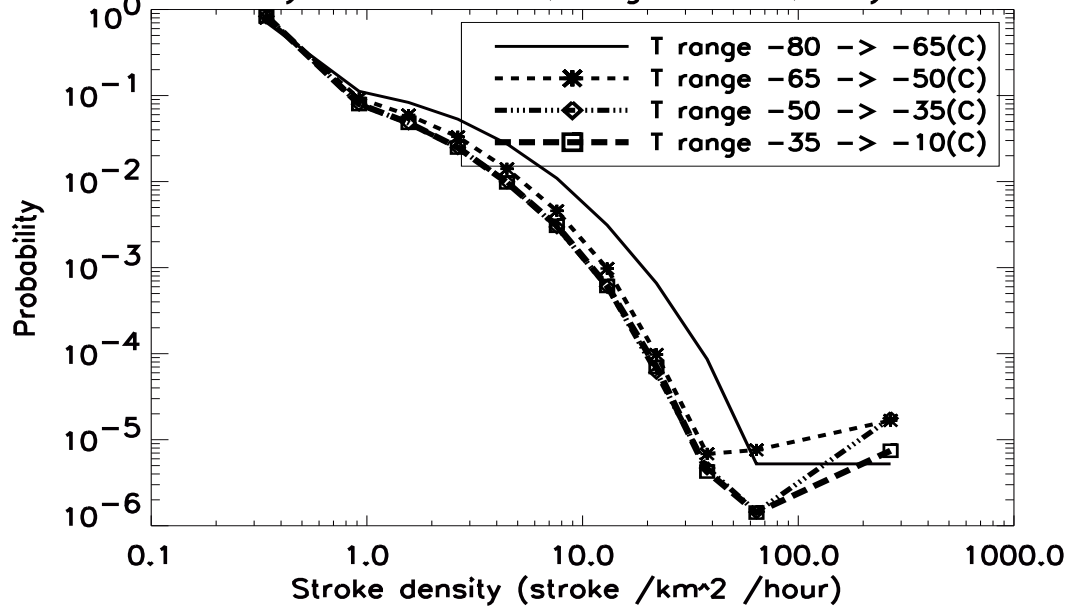


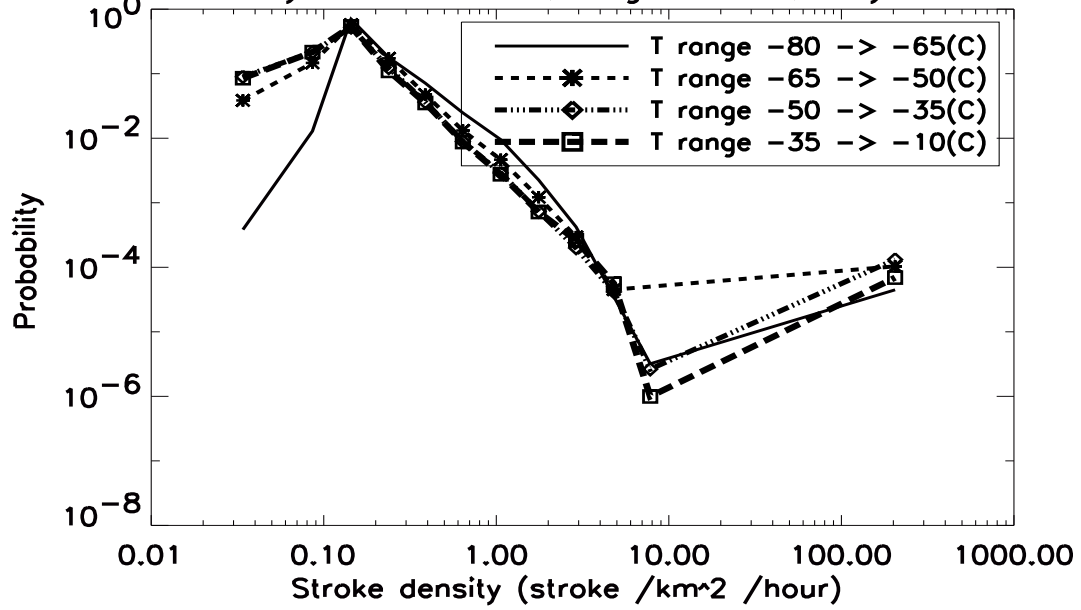
Figure 3: same as figure 2 but for +CGs. Note change in horizontal scale relative to figure 2.

CG stroke density distribution ; Region : 0 ; May to October



(a)

CG stroke density distribution ; Region : 0 ; May to October



(b)

Figure 4: a: Probability of -CG densities to be co-located with CTT in temperature bins. b : same for +CGs.

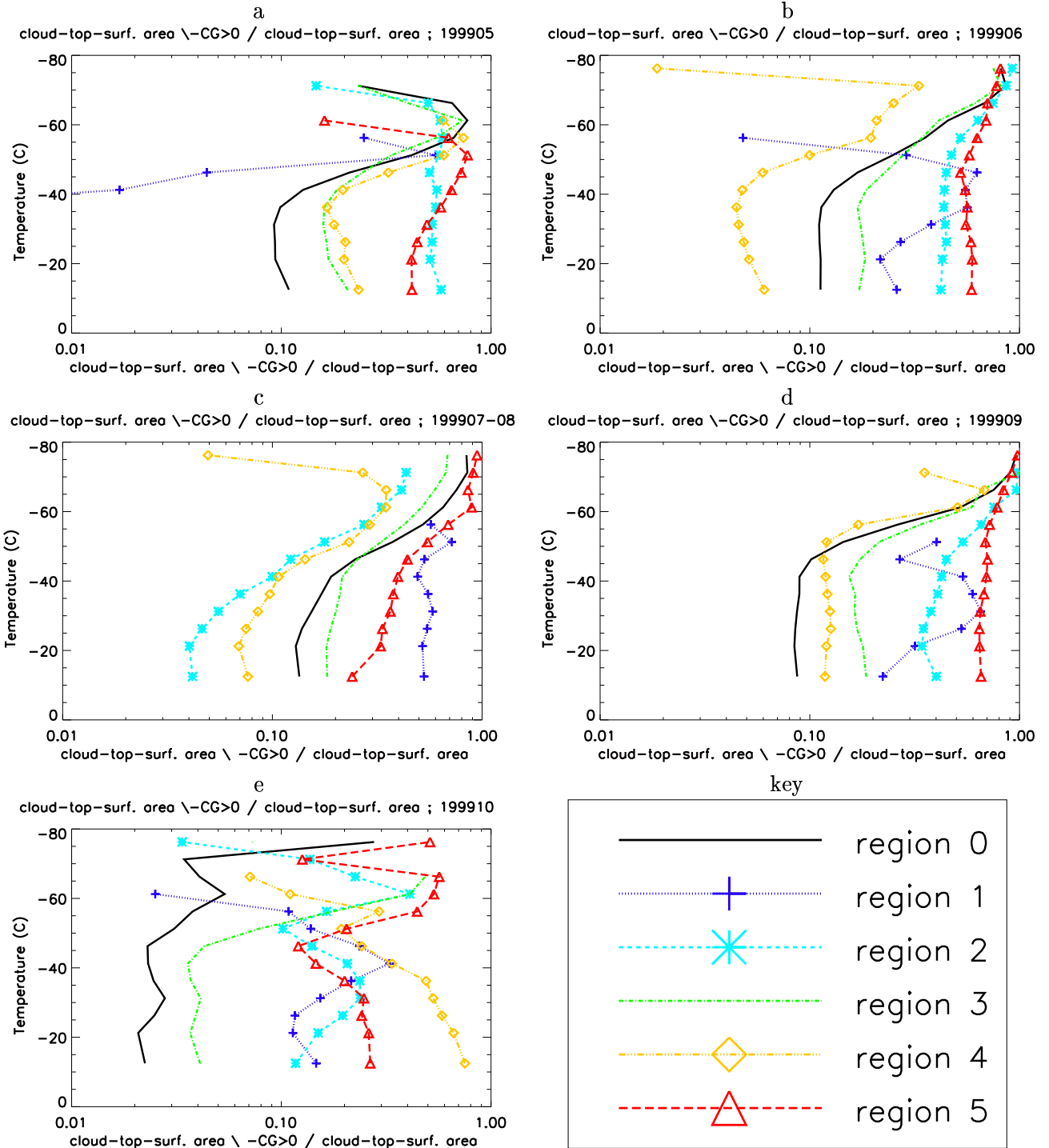


Figure 5: CGP : ratio of the cloud-top-surface area that is in the high-resolution regular temperature bins where the $-CG$ stroke density is non null, to the cloud-top-surface area available in the same temperature bins. Each curve corresponds to a different region (see key). Each graph is for a different month. a : May ; b : June ; c : July-August ; d : September ; e : October ; key : regional identification of curves.

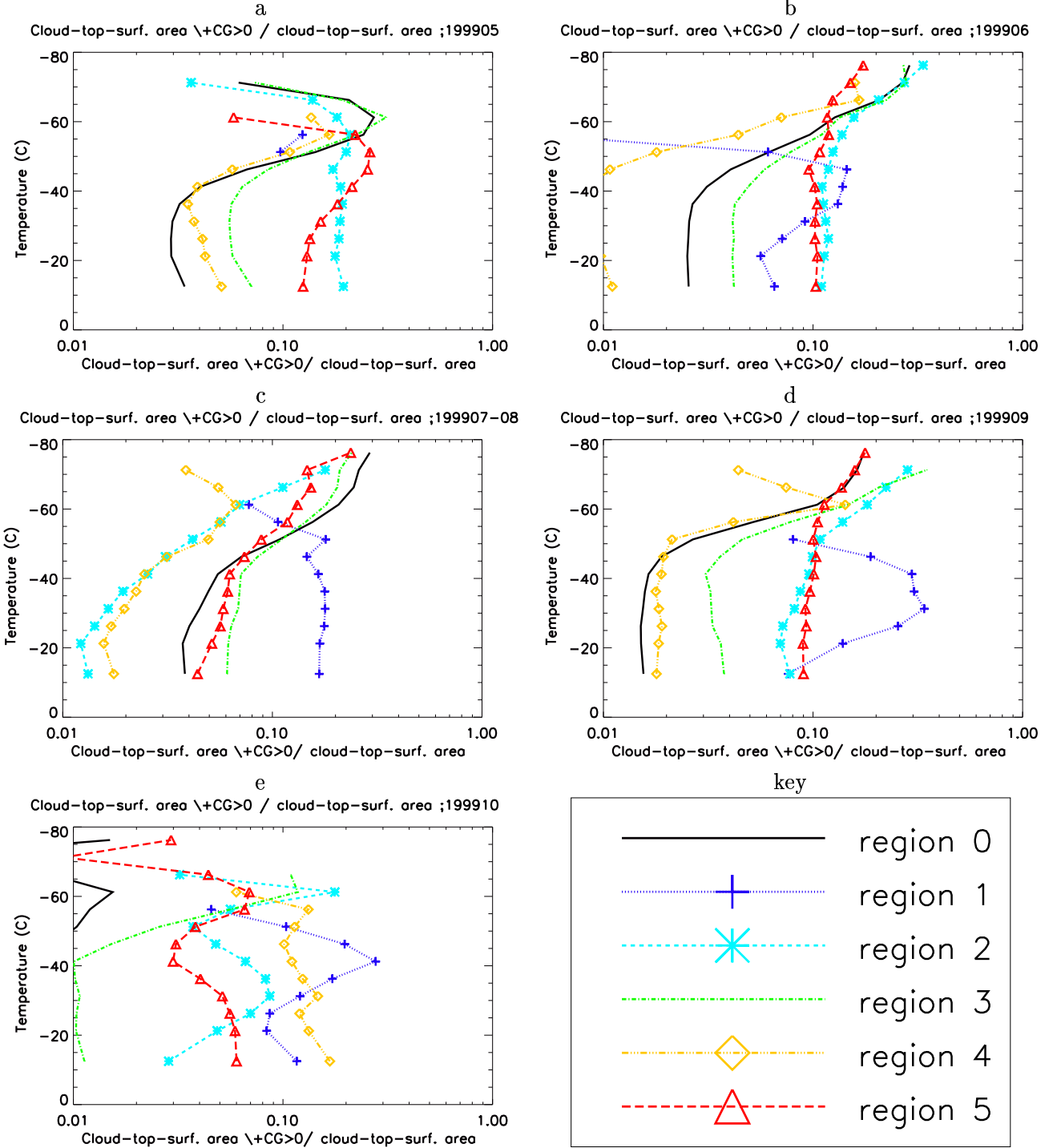


Figure 6: same as figure 5 for +CG

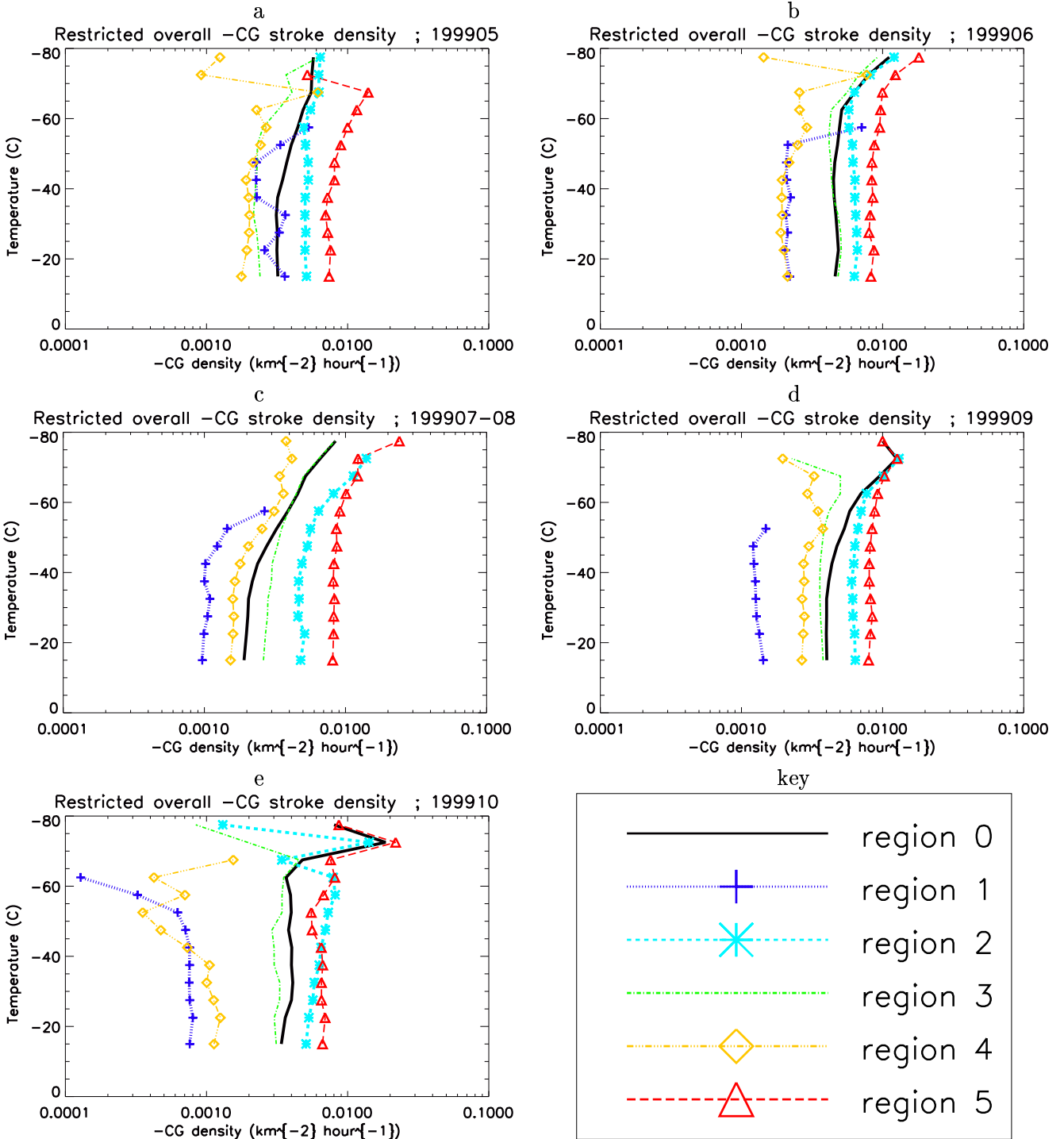


Figure 7: *GSD* : ratio of the number of -CG strokes to the total cloud-top surface where any kind of CG density is non null, observed in the regular temperature bins. Each curve corresponds to a different region (see key). Each graph is for a different month. a : May ; b : June ; c : July-August ; d : September ; e : October ; key : Regional identification of curves.

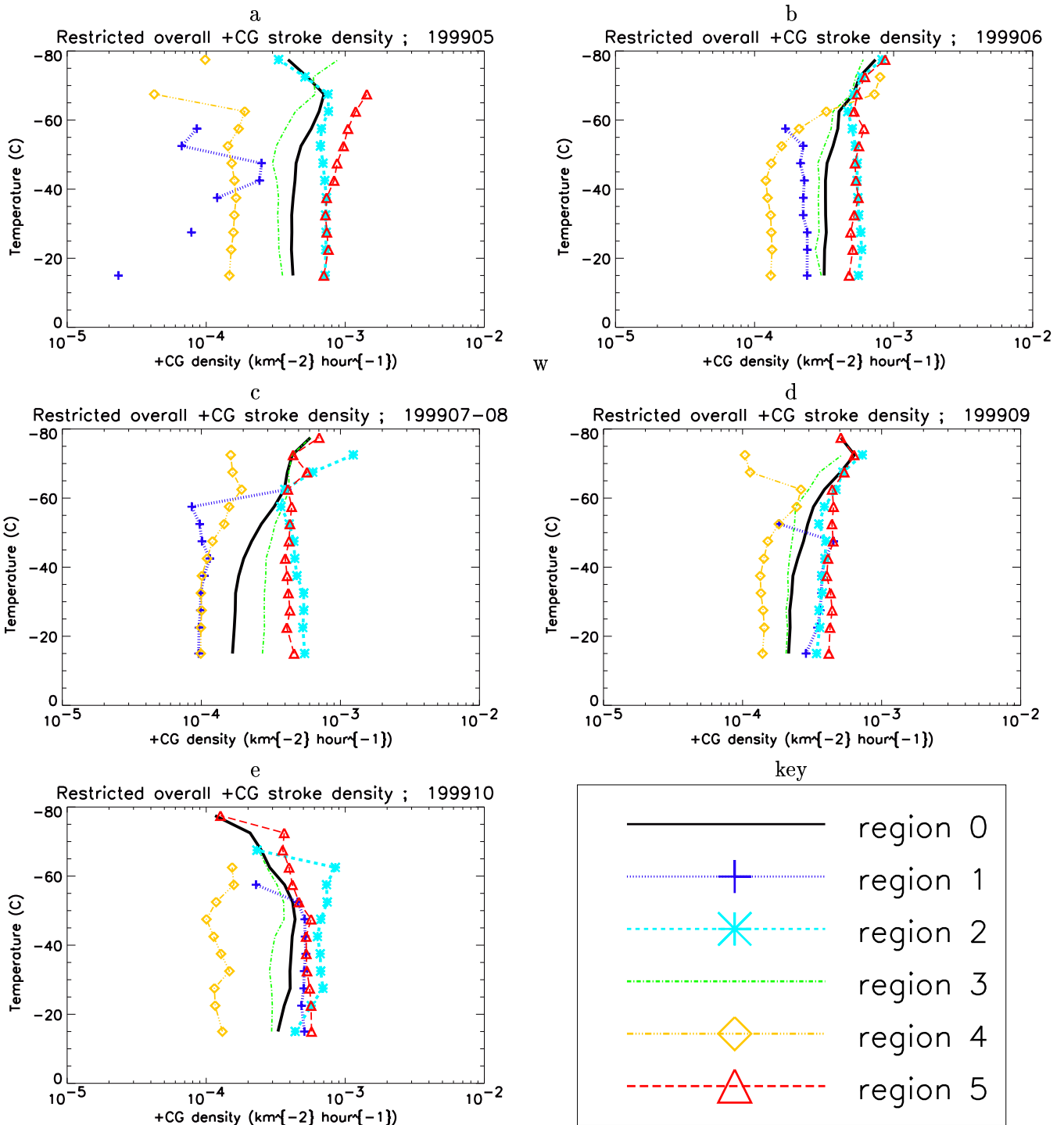


Figure 8: same as figure 7 for +CG

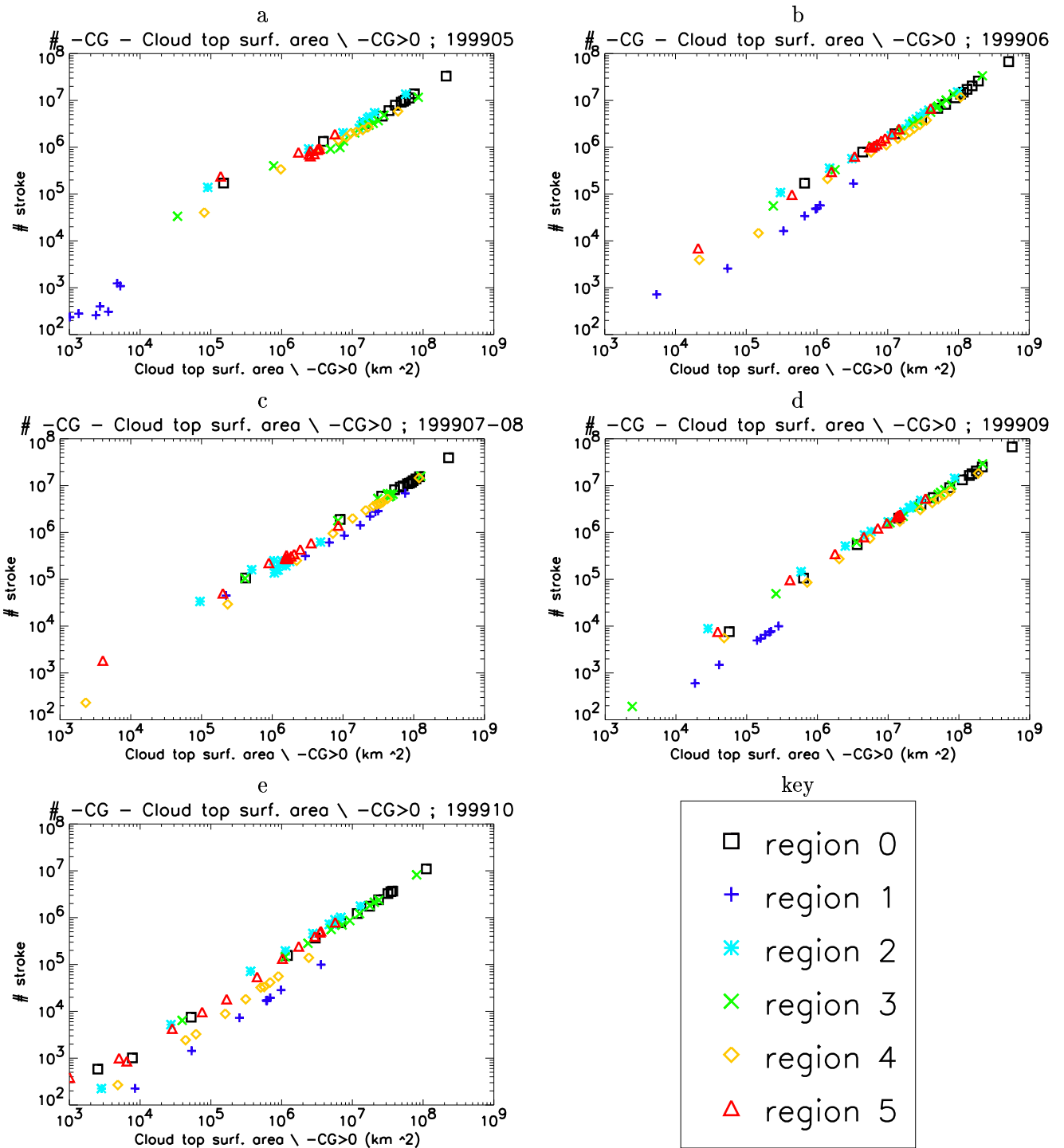


Figure 9: Point pairs ($\#$ -CG strokes, CG thundercloud-top-surface area where the -CG density is non null). Each graph is for a different month. a : May ; b : June ; c : July-August ; d : September ; e : October ; key : regional affiliation of curves

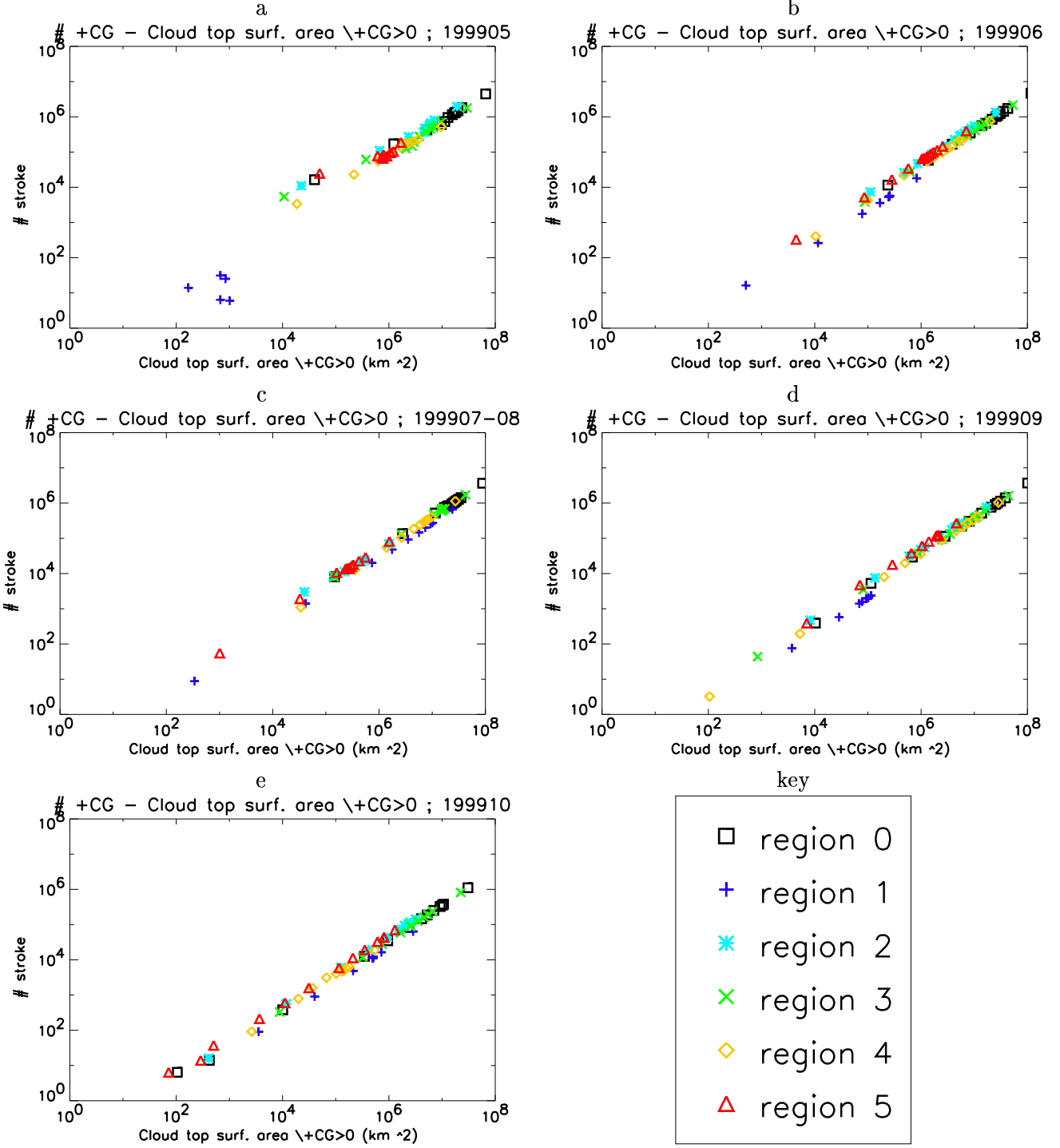


Figure 10: same as figure 9 for +CG

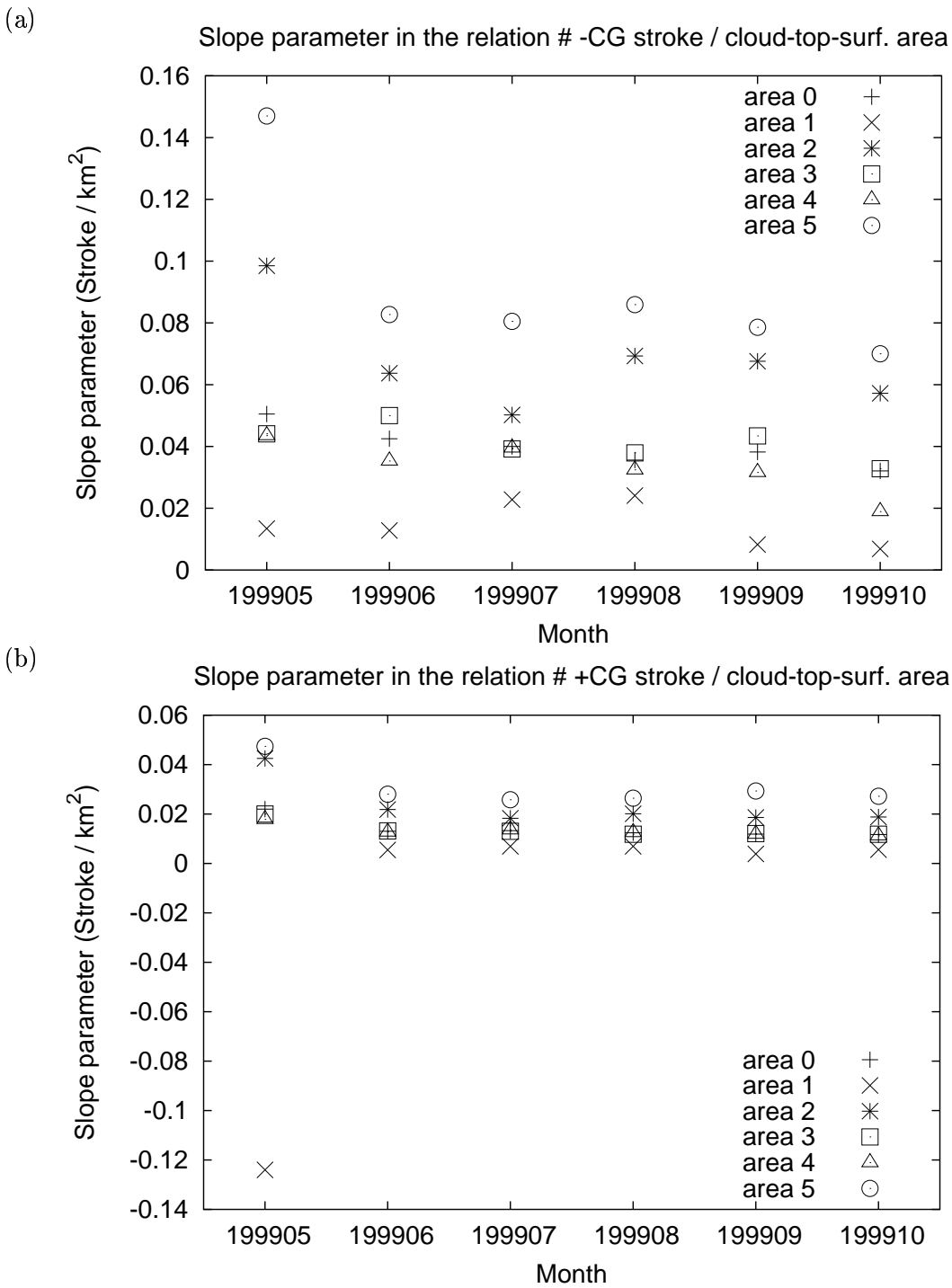


Figure 11: Slope coefficients and intercept values for linear regressions of the number of lightning strokes produced by a given cloud top surface area. Slope coefficients plotted in graphs a and b are in $stroke km^{-2} h^{-1}$ and correspond respectively to -CGs and +CGs.